Supporting Information

Laser-induced graphene-based flexible and all-carbon organic electrochemical transistor

Guozhang Ren,[1] Hua Fan,[1] Linrong Zhang,[1] Shunhao He,[1] Chengcheng Zhu,[1] Kun Gao,[1] Yulong Zhang,[1] Junjie Wang,[1] Xing Kang,[1] Yaxin Song,[1] Zhongyan Gong,[1] Gongqiang Li,[1] Gang Lu,[1]* Hai-Dong Yu[1,2]*

[1]School of Flexible Electronics (Future Technologies), Institute of Advanced Materials, and Key Laboratory of Flexible Electronics, Nanjing Tech University, 30 South Puzhu Road, Nanjing 211816, PR China.

[2]Frontiers Science Center for Flexible Electronics, Xi'an Institute of Flexible Electronics, and Xi'an Institute of Biomedical Materials & Engineering, Northwestern Polytechnical University, 127 West Youyi Road, Xi'an 710072, PR China.

Corresponding authors: Gang Lu, iamglv@njtech.edu.cn; Hai-Dong Yu, iamhdyu@nwpu.edu.cn

Supplementary Figures

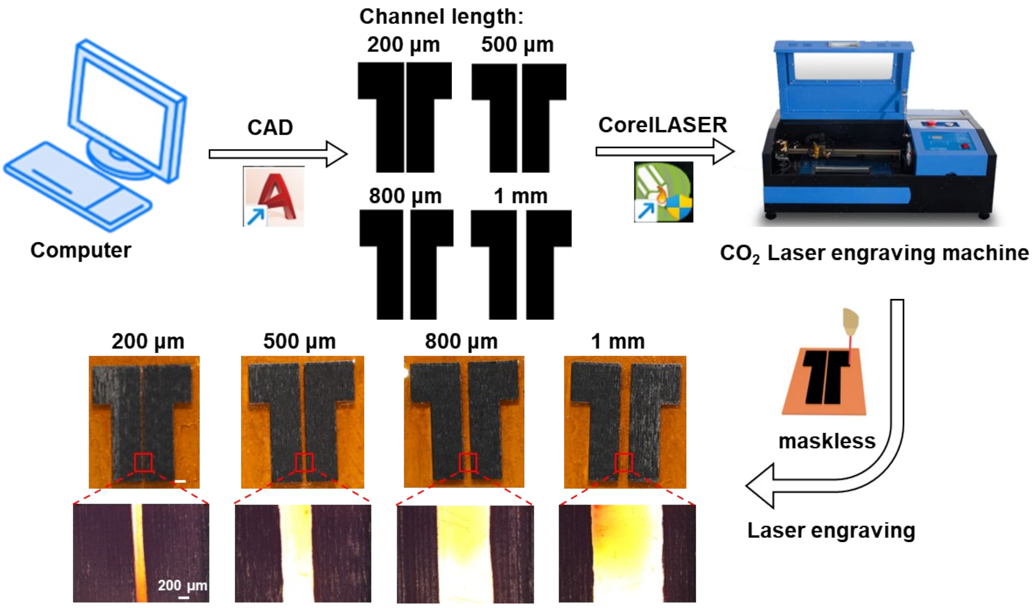

Fig. S1. Methods for preparing LIG electrodes with different channel lengths.

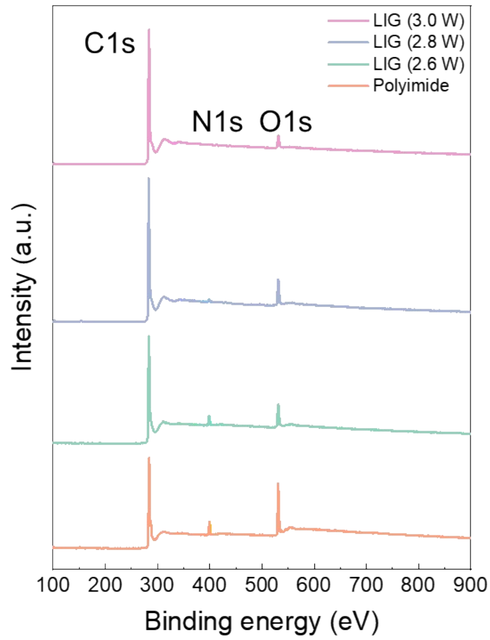

Fig. S2. XPS survey spectra of polyimide and the LIG electrodes prepared at different laser powers.

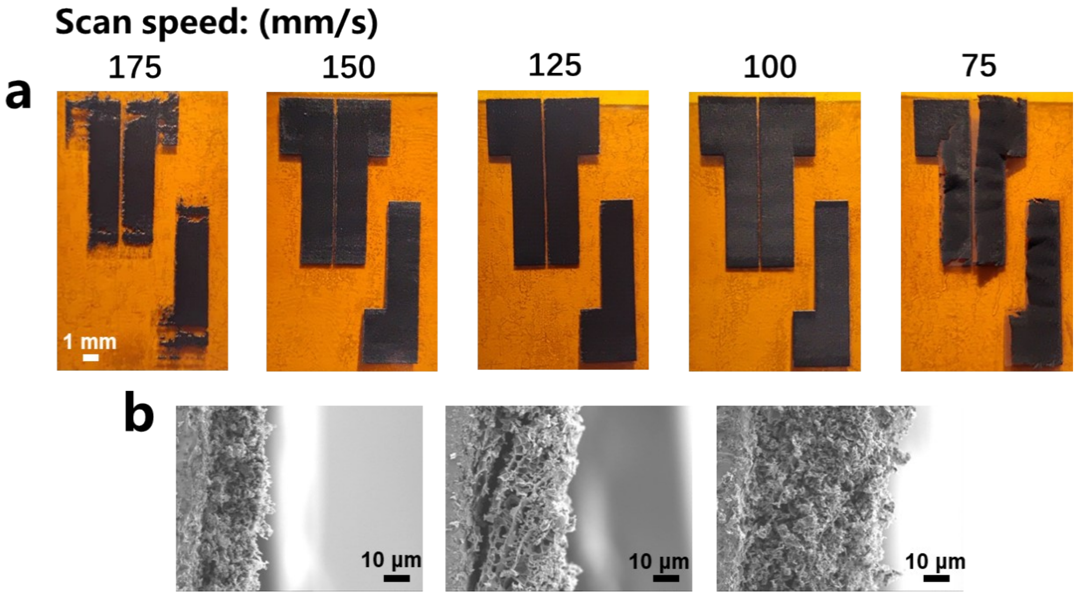

Fig. S3. (a) Photographs of the LIG electrodes prepared at the laser scanning speeds ranging from 75 to 175 mm s^{-1}. (b). SEM cross-sectional images of the LIG electrodes prepared at the laser scanning speeds of 150, 125, and 100 mm s^{-1}.

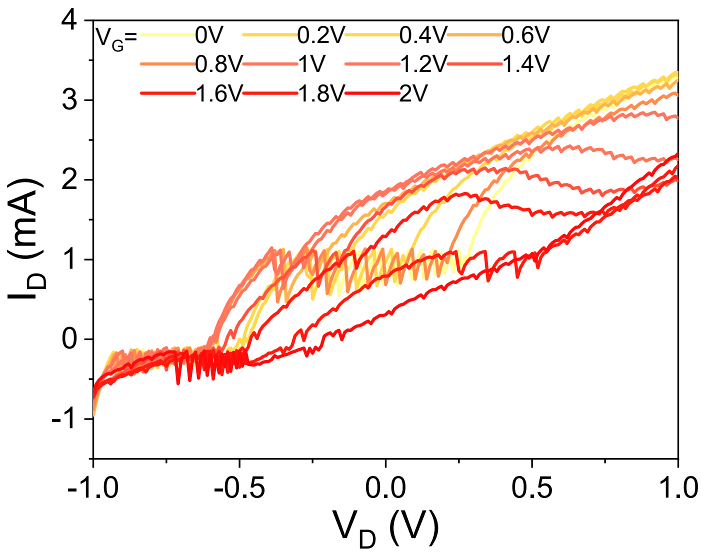

Fig. S4. Output curves of the LIG-OECT based on pristine PEDOT:PSS.

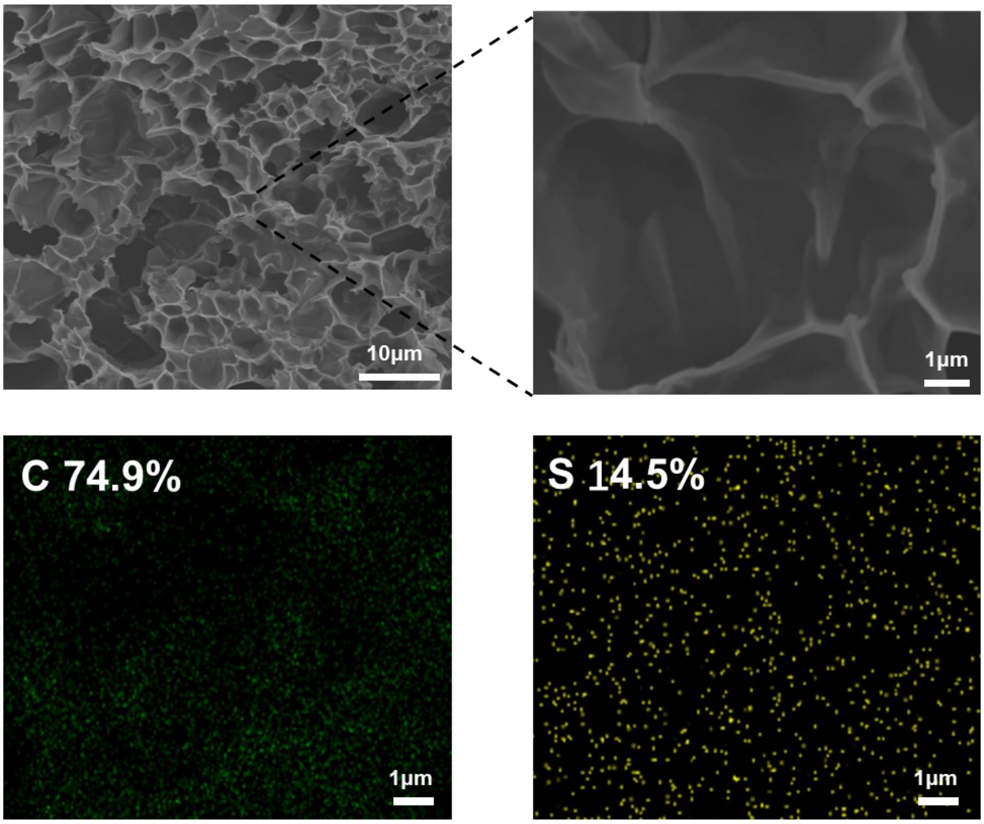

Fig. S5. SEM images and EDS mapping of the PEDOT:PSS coated on LIG surface.

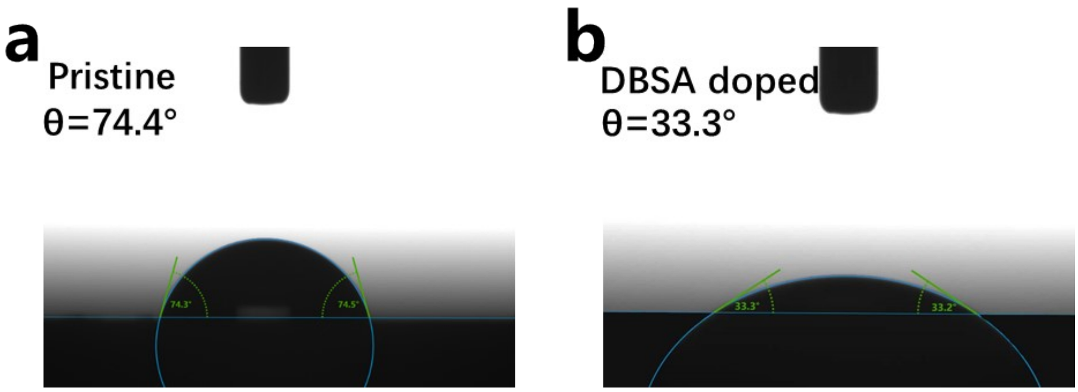

Fig. S6. Water contact angles on the surfaces of (a) pristine and (b) BDSA doped PEDOT:PSS films.

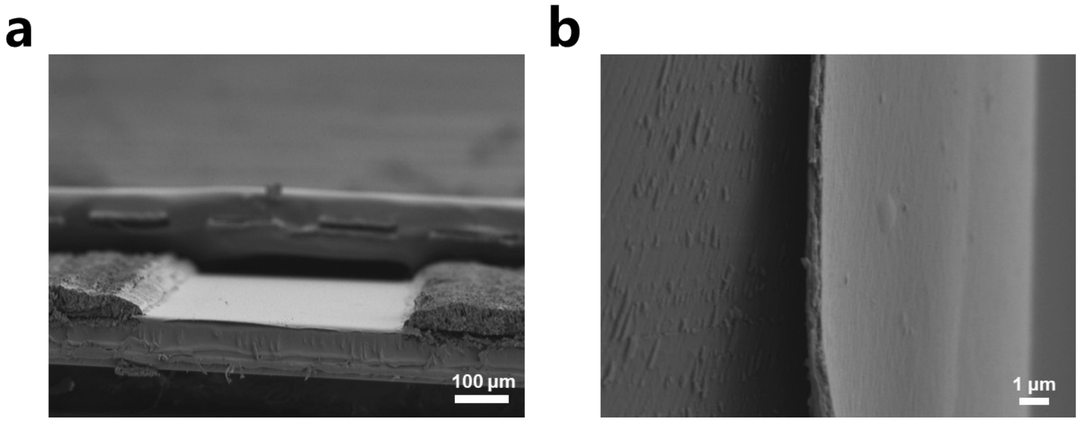

Fig. S7. SEM images of the cross-section of (a) channel LIG-OECT, and (b) PEDOT:PSS layer.

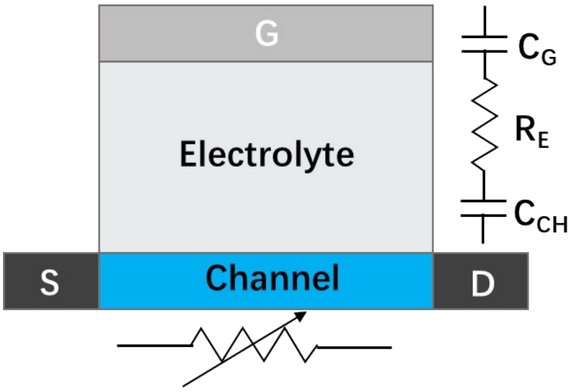

Fig. S8. Equivalent circuit model of OECT.

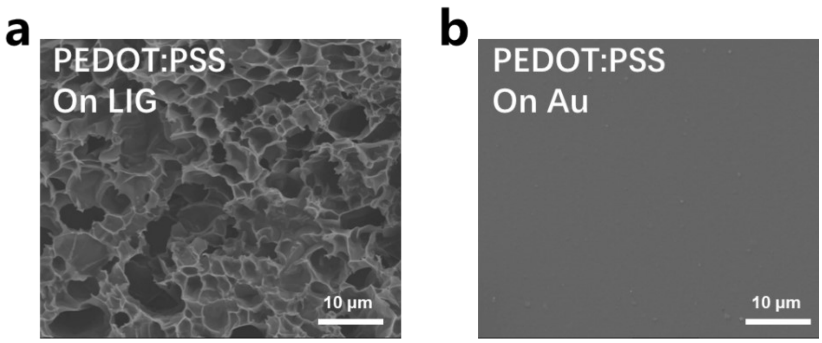

Fig. S9. SEM images of the PEDOT:PSS films on (a) LIG and (b) Au electrodes.

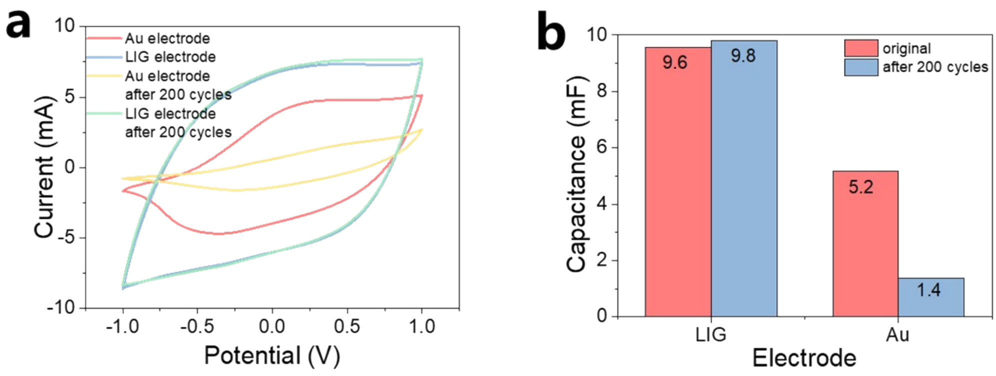

Fig. S10. Capacitance change of the PEDOT:PSS layers on LIG and Au electrodes (a) before and (b) after 200 cycles of CV tests.

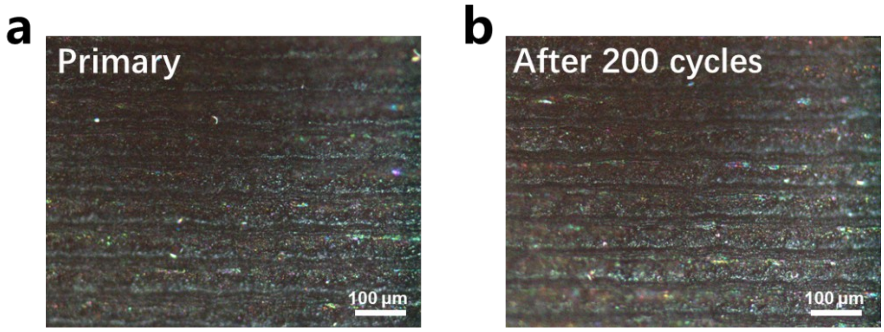

Fig. S11. Optical microscopic images of the PEDOT:PSS layer on LIG electrode (a) before and (b) after 200 cycles of CV tests.

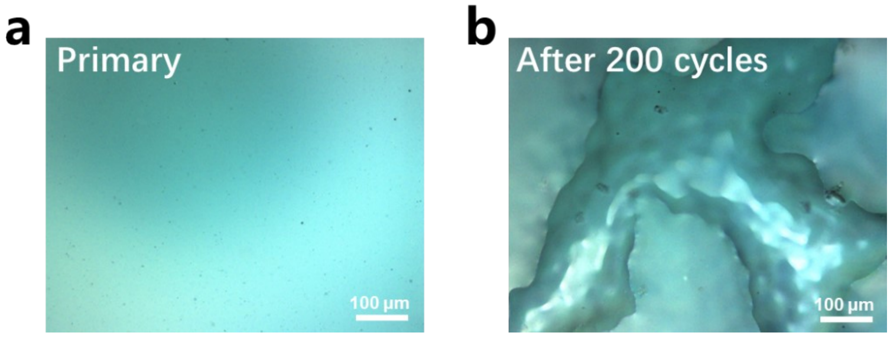

Fig. S12. Optical microscopic images of the PEDOT:PSS layers on Au electrodes (a) before and (b) after 200 cycles of CV tests.

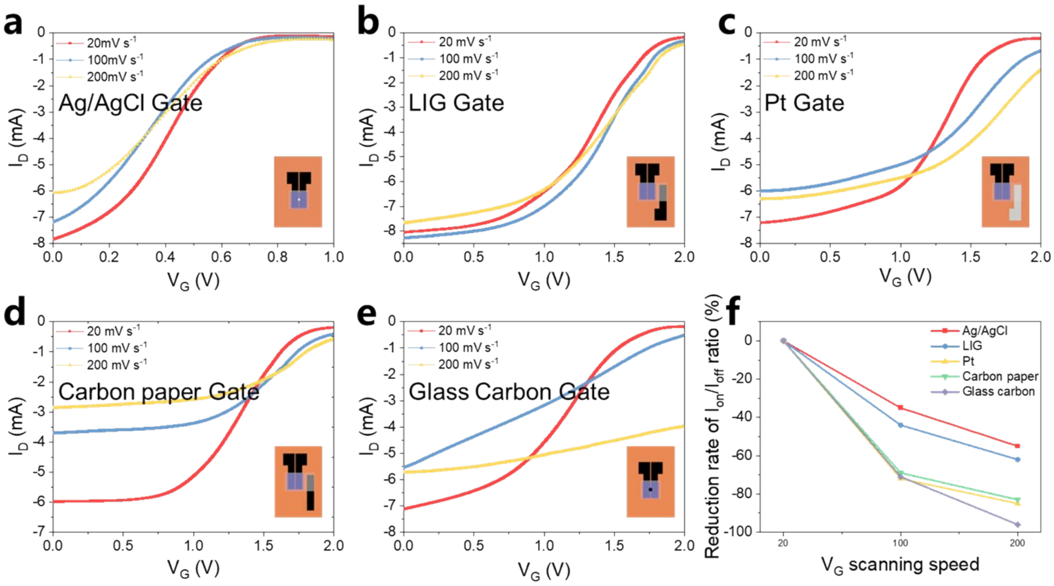

Fig. S13. Transfer curves of LIG-OECT at different gates: (a) Ag/AgCl. (b) LIG. (c) Pt. (d) Carbon paper. (e) Glassy carbon. **f.** The I_{on}/I_{off} ratio decreases with the increase of gate voltage scanning speed

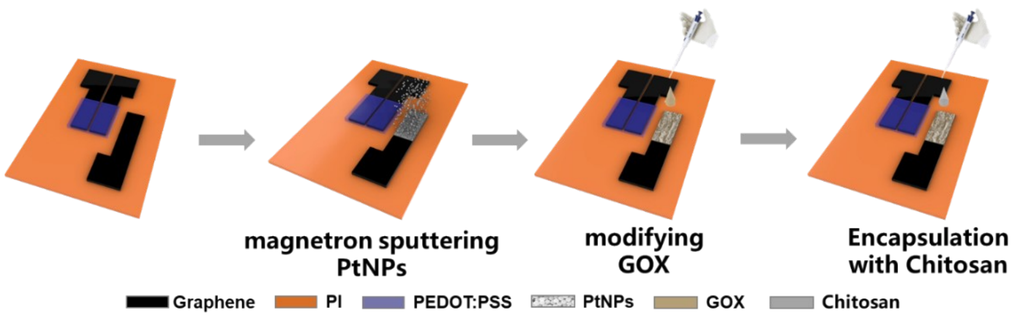

Fig. S14. Schematic diagram of the preparation procedure of the LIG-OECT glucose sensor.

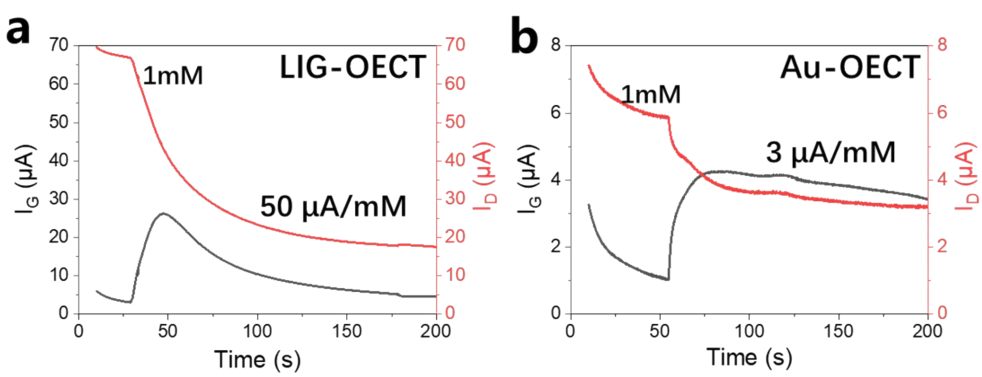

Fig. S15. Response curves of the I_d and I_g of the (a) LIG-OECT and (b) Au-OECT to 1 mM glucose solution.

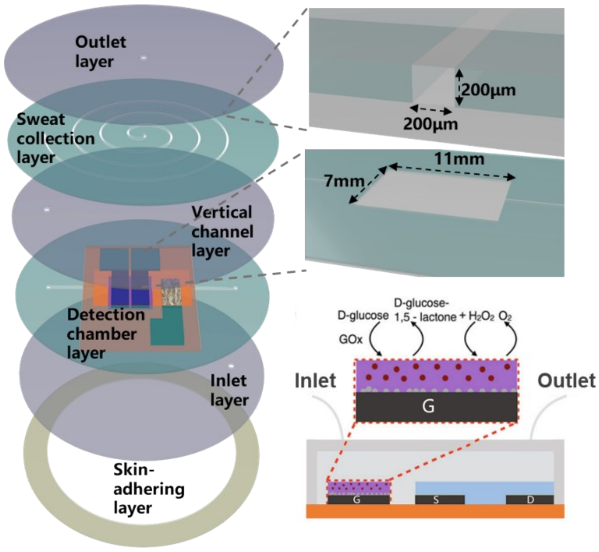

Fig. S16. Schematic diagram of the structure and construction of the microfluidic chip based on LIG-OECT for glucose sensing.

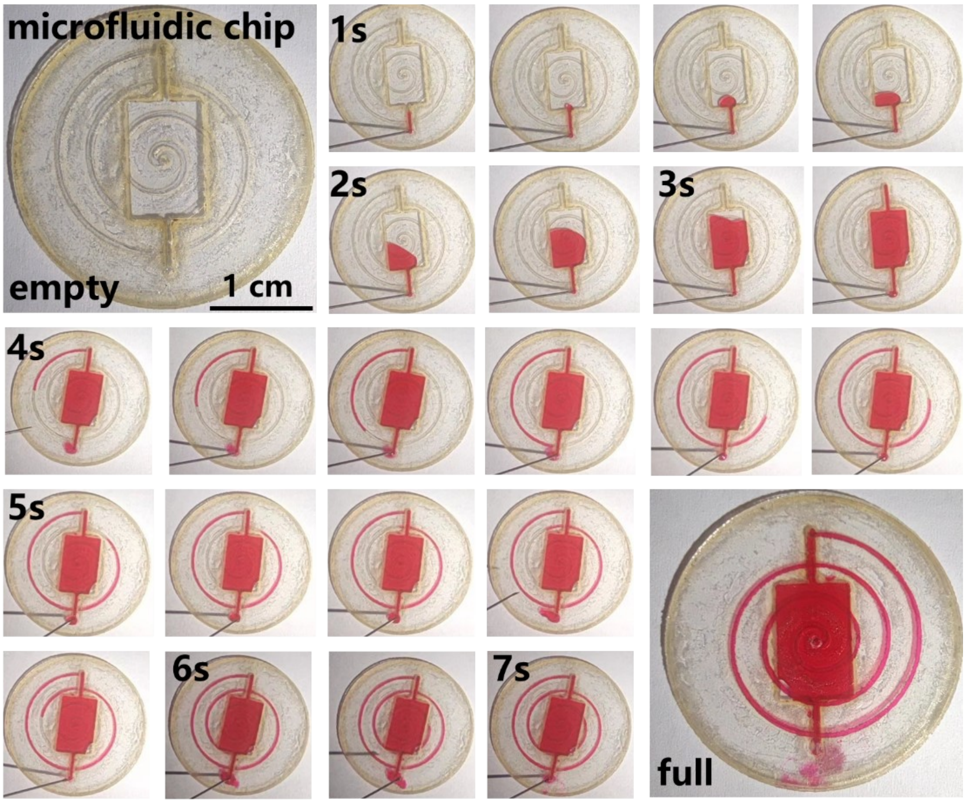

Fig. S17. Photographs showing the flow of red ink in our microfluidic chip.

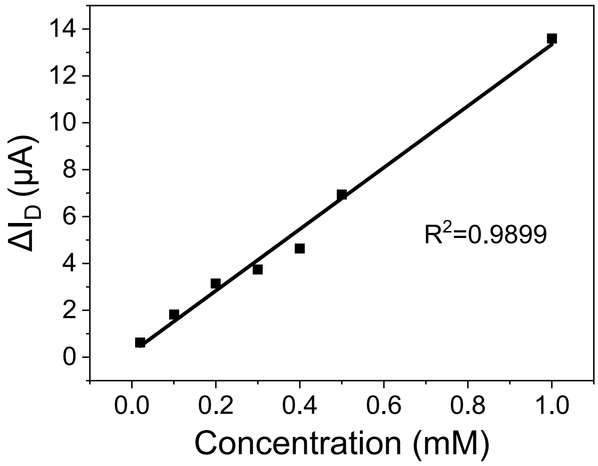

Fig. S18. Linearity of the detection of artificial sweat by the LIG-OECT.

Supplementary Table

Table S1. Performance comparison of glucose detection devices based on OECT.

Channel	Gate electrode	Electrolyte	Detection response time	Detection limit	Ref.
PEDOT:PSS	Pt/Gox	PBS	10 s	100 μM	[1]
PEDOT:PSS	Pt/Gox/Nafion	PBS	≈20 s	100 μM	[2]
PEDOT:PSS	Au/LDH/Gox	PBS	50 s	20 μM	[3]
PEDOT:PSS	Carbon	PBS/Gox	15 s	1μM	[4]
PEDOT:PSS/DBSA/EG	Pt	PBS/Gox	-	1μM	[5]
PEDOT:PSS/DMSO	Graphene	PBS/Gox/Ferrocene	≈70 s	100 nM	[6]
PEDOT:PSS/RTIL/Gox	PEDOT:PSS/RTIL/Gox	PBS	<60 s	100 nM	[7]
PEDOT:PSS/EG	Au/Gox/Chitosan	PBS	15 s	100 nM	[8]
PEDOT:PSS	CHIT/Graphene/Gox/Chitosan	PBS	≈80 s	10 nM	[9]
PEDOT:PSS/AuNPs	Pt/Gox/Nafion	0.1 M NaCl	10 s	10 nM	[10]
PEDOT:PSS/[EMIM][PF6]/DBSA	Pt/Gox/Nafion	0.1 M NaCl	10 s	10 nM	[11]
PEDOT:PSS/DBSA	LIG/PtNPs/Gox/Chitosan	0.1 M NaCl	<5 s	10 nM	This work
PEDOT:PSS	MWCNT-CHIT/PtNPs/Gox	PBS	≈50 s	5 nM	[12]

References

1. Z.-T. Zhu, J. T. Mabeck, C. Zhu, N. C. Cady, C. A. Batt and G. G. Malliaras, *Chem. Commun.*, 2004, **40**, 1556-1557.
2. A. Ait Yazza, P. Blondeau and F. J. Andrade, *ACS Appl. Electron. Mater.*, 2021, **3**, 1886-1895.
3. I. Gualandi, M. Tessarolo, F. Mariani, D. Arcangeli, L. Possanzini, D. Tonelli, B. Fraboni and E. Scavetta, *Sensors*, 2020, **20**, 3453.
4. D. A. Bernards, D. J. Macaya, M. Nikolou, J. A. DeFranco, S. Takamatsu and G. G. Malliaras, *J. Mater. Chem.*, 2008, **18**, 116-120.
5. S. Khan, S. Ali, A. Khan, B. Wang and A. Bermak, *IEEE Sens. J.*, 2021, **21**, 4167-4175.
6. S. Demuru, C.-H. Huang, K. Parvez, R. Worsley, G. Mattana, B. Piro, V. Noël, C. Casiraghi and D. Briand, *ACS Appl. Nano Mater.*, 2022, **5**, 1664-1673.
7. S. Y. Yang, F. Cicoira, R. Byrne, F. Benito-Lopez, D. Diamond, R. M. Owens and G. G. Malliaras, *Chem. Commun.*, 2010, **46**, 7972-7974.
8. J. Li, F. Madiyar, S. Ghate, K. S. Kumar and J. Thomas, *Nano Res.*, 2023, **16**, 3201-3206.
9. C. Liao, M. Zhang, L. Niu, Z. Zheng and F. Yan, *J. Mater. Chem. B*, 2013, **1**, 3820-3829.
10. L. Zhang, L. Wang, S. He, C. Zhu, Z. Gong, Y. Zhang, J. Wang, L. Yu, K. Gao, X. Kang, Y. Song, G. Lu and H.-D. Yu, *ACS Appl. Mater. Interfaces*, 2023, **15**, 3224-3234.
11. L. Wang, Q. Sun, L. Zhang, J. Wang, G. Ren, L. Yu, K. Wang, Y. Zhu, G. Lu and H.-D. Yu, *Macromol. Rapid Commun.*, 2022, **43**, 2200212.
12. H. Tang, F. Yan, P. Lin, J. Xu and H. L. W. Chan, *Adv. Funct. Mater.*, 2011, **21**, 2264-2272.